Applied Surface Science 599 (2022) 153976

Contents lists available at ScienceDirect

Applied Surface Science

journal homepage: www.elsevier.com/locate/apsusc

Full Length Article

# Theoretical and experimental study on plasma-induced atom-migration manufacturing (PAMM) of glass

Shaoxiang Liang, Linfeng Zhang, Hui Deng *

*Department of Mechanical and Energy Engineering, Southern University of Science and Technology, Shenzhen, Guangdong 518055, PR China*

ARTICLE INFO

*Keywords:*
Plasma
Atomic and close-to-atomic scale manufacturing
Finishing
Atom migration
Roughness

ABSTRACT

Optical manufacturing plays an important role in various fields, such as optical lenses, telescopes, and laser optics. Generally, traditional optical manufacturing techniques are all subtractive processes based on the micro-shearing effect between the tool and surface protrusions. This paper reports a plasma-induced atom migration manufacturing (PAMM) process, which is a nonsubtractive finishing approach by which angstrom level surface roughness of fused silica has been successfully achieved. Inductively coupled plasma (ICP), which is characterized by high temperature and high radical density, is used as the tool of PAMM. After obtaining instantaneous plasma energy input on the fused silica surface, the peak site atoms migrate to the valley sites, thereby reducing the roughness. According to the energy minimization principle, this migration process continues until an ultra-smooth surface with reduced surface energy is formed. Atomic-scale molecular dynamics simulations were performed to clarify the microscopic mechanisms of PAMM, and experiments were conducted to verify its smoothing capability. The roughness of a ground silica surface was drastically reduced from *Sa* 391 nm to *Sa* 0.16 nm. This study demonstrates the feasibility of the PAMM as an alternative approach for atomic-level surface manufacturing.

## 1. Background

At present, the base approach for optical manufacturing is computer-controlled optical surfacing (CCOS) technology [1]. Based on the pre-measurement of error information and the well-developed dwell time algorithm, CCOS enables selective and quantitative removal of surface components with low spatial frequency error. As mathematical models are adopted in CCOS, the polishing process exhibits a high degree of certainty. Currently, it has been widely used in optical manufacturing to improve the form accuracy [2]. In recent decades, some ultraprecision optical manufacturing technologies derived from CCOS have been proposed and commercially utilized, such as magnetorheological finishing (MRF) and ion beam finishing (IBF).

MRF is carried out under the action of a directional magnetic field, and the magnetorheological fluid drives the polishing powders to abrade the surface and achieve material removal by the shear effect. MRF is capable of effectively removing subsurface damage induced by CCOS, reducing surface form error and achieving subnanometre surface roughness [3]. IBF technology uses inert gas ions to bombard the workpiece surface to transfer kinetic energy. With appropriate ion energy, the surface material can be removed by sputtering. Compared with CCOS and MRF, IBF technology has a more stable removal function [4,5]. Based on the control of ion energy and other parameters, atomic-scale material removal can be realized by IBF. However, IBF has a limited ability to improve high-frequency surface roughness.

With the rapid development of manufacturing technologies, atomic and close-to-atomic scale manufacturing (ACSM), in which material removal, migration and addition occur, is becoming an attractive field [6,7]. The manufacturing of atomic surfaces is an important area for the development of ACSM. However, in conventional surface finishing approaches, there are many constraints to achieve atomic-level surface roughness. The core constraint is that the minimum material removal volume of subtractive manufacturing approaches is much larger than that of atoms, which is the minimum constituent unit of the material. Therefore, it is difficult to achieve the efficient conversion of roughness from the nanometre level to the angstrom/subangstrom level.

It could be easily understood from the calculation formula of roughness that the most fundamental approach to obtain a smooth surface is to reduce the height difference between the peak sites and the valley sites on the surface. Traditional polishing technology is usually

* Corresponding author.
*E-mail address:* dengh@sustech.edu.cn (H. Deng).

https://doi.org/10.1016/j.apsusc.2022.153976
Received 24 March 2022; Received in revised form 1 June 2022; Accepted 13 June 2022
Available online 15 June 2022

based on the shearing effect between the tool and surface protrusions, and surface smoothing is realized by selective removal of the protrusions. However, from the definition of surface finishing, material removal is not the necessary and sufficient condition to obtain a smooth surface. The surface can be definitely smoothed if the atoms on the peak sites can migrate to the valley sites.

In 1990, IBM realized the migration manipulation of a single atom based on scanning tunnelling microscopy (STM) [8]. In this process, the tip of the probe captures and moves the target atoms and then places them in the target position. In recent years, this technology has also realized batch manufacturing of atomic structures [9]. Similarly, atomic manipulation technologies based on atomic force microscopy (AFM) [10] and scanning transmission electron microscopy (STEM) [11] have also been reported. These probe-based atomic manipulation technologies realized ultraprecision manufacturing at the atomic scale. However, the application range of atomic manipulation technology is limited to the nanometre scale and cannot complete batch atomic migration at the micrometer or even millimetre scale. Therefore, probe-based atomic manipulation technologies present obstacles in the manufacturing of large-scale ultrasmooth surfaces.

From the perspective of atomic interactions, the process of atomic migration is divided into the failure of atomic interactions, the movement of atoms and the reconstruction of atomic interactions. In STM atomic manipulation technology, these processes can be completed by adjusting the potential energy of the probe [8]. For the cross-scale migration of quantities of atoms, the key process is instantaneous energy transfer on the surface. Energy beams can be used as a medium for this transmission; therefore, energy beam-induced atomic migration manufacturing technology is developing. According to the different energy sources, the energy beam can be divided into laser beam, electron beam, ion beam and plasma beam. Since the 1980 s, laser beam-induced atomic migration manufacturing [12–14] has been gradually applied to surface polishing and damage recovery of optical, semiconductor and metal components. Electron beam-induced atomic migration manufacturing [15–18] technology has been widely used in the surface polishing of metal components. This technology has been applied for production of components for use in many fields, such as artificial knee joint parts and surgical tools [19], metal dentures and thin osteotomy blades [20], 3D printing components [21], and metal moulds [22,23]. Ion beam-induced atomic migration manufacturing [24–26] technology is applied to precision optical elements and small metal parts. In the above process, the energy beam achieves the micromelting of the outermost layer on the workpiece surface, and the atoms migrate to obtain ultrasmooth surfaces with nanoscale or even subnanoscale roughness [27].

Plasma beam-induced atomic migration manufacturing research was first reported in 2015 [28]. After microplasma beam irradiation on the grey iron surface, the rough rusty surface became smooth. In recent years, arc plasma has made several advances in metal part polishing [29]. On the surface of SUS304 steel, the Ra roughness decreased from 4.07 μm to 0.46 μm [30]. On the surface of AISI 304 stainless steel, the Ra roughness decreased from 5.11 μm to 0.41 ± 0.05 μm [31]. However, after arc plasma irradiation, there was no polishing effect on the FCD500-7 steel surface. Moreover, obvious ripples appear on the surfaces of SKD61 and SUS420J2 steel, resulting in increased surface roughness [30]. This is because the arc plasma is a typical microarea discharge, so its temperature distribution is extremely uneven, and there is an obvious gas explosion in the arc area. In addition, the current machining accuracy of arc plasma can only reach the submicron level, and it is difficult to apply to optical components due to subsurface stress problems.

This study introduces a surface atomic migration manufacturing technology based on inductively coupled plasma (ICP). ICP is a typical strong ionized and equilibrium plasma that exhibits the characteristics of high temperature and high particle concentration. Its temperature can be adjusted within the range of hundreds to thousands of degrees. Compared with an arc, an ICP can maintain a more uniform and stable glow discharge mode. Therefore, ICP is expected to serve as an effective medium for surface atomic migration at the millimetre scale. In this study, plasma-induced atomic migration manufacturing (PAMM) technology was proposed for surface smoothing. The atomic migration mechanism in the PAMM process was studied by molecular dynamics simulation, and the core control factors were revealed. Then, based on the feasibility of the polishing experiment, the roughness and surface morphology evolution of PAMM were studied, and the ultimate roughness on the fused quartz component was explored.

## 2. Principle and experimental setup of PAMM

Fig. 1 (a) shows a schematic diagram of the PAMM polishing process based on ICP plasma. The critical process of PAMM is the instantaneous energy transfer to the workpiece surface by ICP, mainly through three modes: thermal convection, heat conduction and thermal radiation. Since the temperature of ICP plasma is high and the surface temperature of fused silica is low, the nonuniformity of temperature leads to the occurrence of thermal convection, so the heat is transmitted to the fused silica surface through gas. A large number of high-speed particles in ICP can directly collide with fused silica surface atoms to transmit energy. ICP is a strong ionization plasma that contains many excited atoms and molecules. The excited state particles release energy by radiation during the de-excitation process, and the surface atoms can absorb this energy.

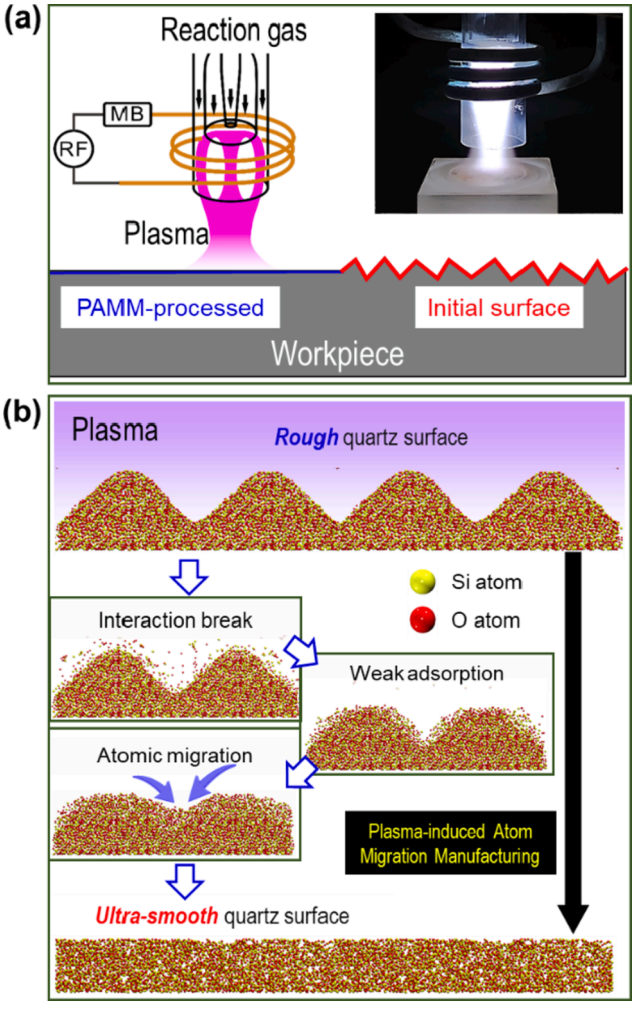


**Fig. 1.** a) Schematic diagram of PAMM polishing (the insert is the PAMM setup on the fused silica surface); b) schematic diagram of the PAMM smoothing process on the fused silica surface.

Based on these energy transfer pathways, the surface atoms absorb sufficient energy. Thus, the bonding between atoms is broken so that atomic migration can occur. The insert shows the experimental setup for PAMM polishing on the fused silica surface by ICP, which is mainly composed of an RF power supply, copper inductor coil, quartz torch tube, alumina ceramic sample table and three-axis CNC (computerized numerical control) motion system. The quartz torch tube is fixed at the centre of the induction coil and consists of two coaxial quartz tubes. The inner tube supplies ignition gas (Ar, 1.5 slm), and the outer tube supplies cooling gas (Ar, 18.5 slm) to prevent the fused quartz torch tube from melting at high temperature, simultaneously stabilizing the ICP plasma beam. Through the CNC motion platform, the fused silica sample can be surface-treated in a fixed and complete manner.

The excited state particles release energy by radiation during the mechanism, including bond breaking, adsorption, movement and bond formation. After absorbing enough energy, the covalent bonds between Si/O atoms on the fused silica surface break to form free atoms or atomic clusters. These free atoms and clusters are adsorbed on the surface only by van der Waals interactions. According to the principle of energy minimization, free atoms or clusters migrate on the surface to find low-energy sites. When the free atoms and clusters in the high point position fill the low point position on the surface, the surface area of fused silica decreases; thus, the surface energy decreases. The above migration process continues until the surface reaches a stable low-energy state: that is, to obtain an ultrasmooth surface. Since the plasma energy input only acts on several surface layers of the material instantaneously, this process is equivalent to atomic rearrangement on the fused silica surface under ICP plasma irradiation. Finally, the atomic-scale ultrasmooth surface is obtained based on the "atomic migration effect".

In this study, 40 mm × 40 mm × 5 mm quartz samples were used to study the polishing mechanism and process of PAMM. Before the experiment, all samples were ultrasonically cleaned with ultrapure water and high purity ethyl alcohol (99.5%) and then dried with nitrogen (99.999%). In this study, an ultra-precision balance (METTLER CC-3372–02) was used to measure the weight change of fused silica samples during PAMM. The free radical composition in ICP plasma was measured by an optical emission spectrometer (OES, Ocean Optics USB4000) with a wavelength resolution of 0.2 nm. The temperature distribution on the fused silica surface during PAMM was observed and recorded by a thermal imaging spectrometer (FLIR T660). The surface morphology was observed by laser scanning confocal microscopy (LSCM, Keyence VK-X1000), while the surface roughness was measured by scanning white light interferometry (SWLI, Taylor Hobson M112-4449–02 CCI HD) and atomic force microscopy (AFM, Bruker Edge). The profile and roughness distribution of the samples at the millimetre scale were measured by a stylus profiler (SURFCOM NEX 031 DX-12).

The composition of free radicals in ICP plasma (RF power 1,500 W) was determined by emission spectroscopy, as shown in Fig. 2 (a). The optical fibre probe was fixed at a distance of approximately 200 mm from the torch centre, and the emission spectrum was recorded with a 60 ms constant integration time for all collected data. The wavelength of the emission line represents the element type, and the emission intensity represents the number density of free radicals. Since the PAMM process uses pure Ar without adding any other elements as the reaction gas, many peaks with strong intensity corresponding to Ar excitation atoms can be detected as well as some weak peaks derived from ambient nitrogen molecules. The broad spectrum is considered originated from bremsstrahlung radiation.

The setup consists of an RF power supply (40.68 MHz), an impedance matcher, a copper inductance coil, a quartz torch, a water-cooling circulation system, and so forth. The quartz torch, which was fixed in the centre of the inductive coil, was composed of two coaxial quartz tubes; the ignition gas (Ar, 1.5 sccm) was supplied through the inner tube (ID: 16 mm), and cooling gas (Ar, 18.5 sccm) was supplied through the outer tube (ID: 20 mm) to prevent the tube from melting and stabilize the plasma torch. Under the cooperation of the above components and parts,

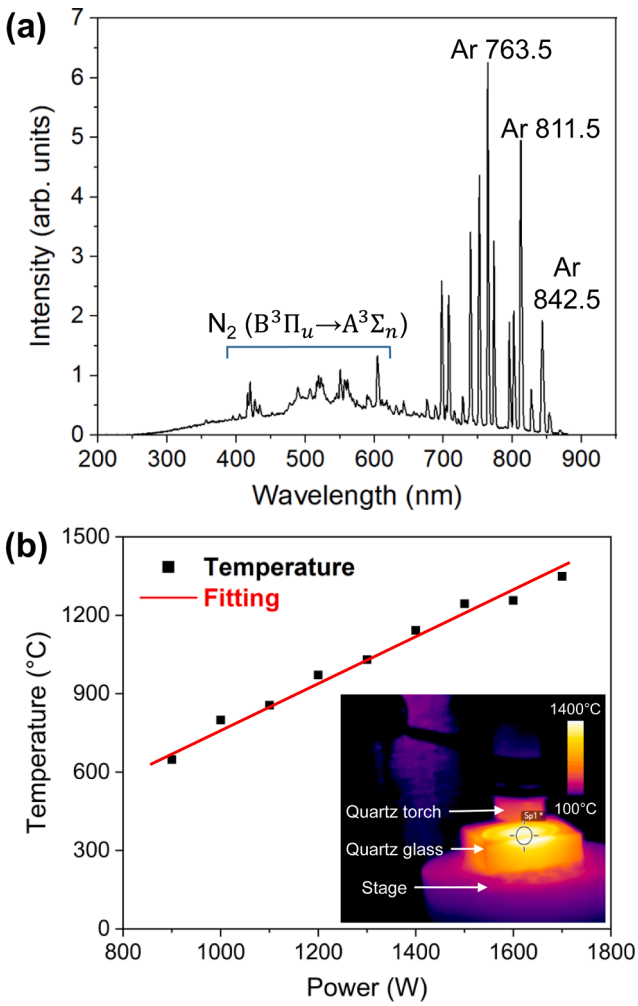


**Fig. 2.** a) OES spectrum of ICP (1,500 W); b) variation in fused silica surface temperature with RF power during the PAMM process (the inset is the heatmap of the fused silica surface during the PAMM process).

plasma was generated in the quartz torch. In the PAMM process, the sample was placed on a wafer holder made of high temperature resistant aluminium oxide ceramics.

The temperature of the fused quartz surface at different RF powers was measured, and the results are shown in Fig. 2 (b). The research shows that the surface temperature has a linear relationship with RF power. By adjusting the RF power, the surface temperature of fused quartz can be roughly controlled from 600 to 1,400 °C. The insert shows the thermal image of fused quartz during PAMM. Since the temperature in the circular region below the plasma torch is the highest, the temperature in this region was recorded, and the average value was taken as the surface temperature. When the RF power was 1,500 W, the average temperature of the fused quartz surface was 1,200–1,300 °C.

## 3. Theoretical research based on molecular dynamics simulation

In this study, large-scale atomic/molecular parallel simulation (LAMMPS) [32] software was used to calculate and analyse the PAMM process of fused silica at the atomic scale based on molecular dynamics (MD) simulation. The simulation results were visualized in Visual Molecular Dynamics (VMD) [33] and Open Visualization Tool (OVITO) [34] software. The interaction between atoms in covalently bonded molecules depends not only on the distance between atoms but also on the bonding direction between atoms. Therefore, the influences of

surrounding atoms must be considered in calculating the interaction between atoms in fused silica. According to the concept of bond order (i.e., bond strength) in quantum mechanics, Tersoff proposed the Tersoff potential function [35] from basic quantum mechanics theory. The Tersoff potential function describes the relationship between bond order and the surrounding environment and proposes a Morse-type atomic interaction model, which can accurately describe the interaction between covalent bonds. To obtain more accurate calculation results, the three-body Tersoff potential is applied to the complex covalent bond system in fused silica [36].

Fig. 3 (a) shows the initial height distribution model of the fused silica surface. In this study, a continuous rough surface composed of hemispherical bulges and pits is designed. The Sa roughness of the initial surface is 1.38 nm. The bottom of the model is 16.7 nm × 16.7 nm, which consists of 31,509Si atoms and 63,019O atoms, and the density is 2.21 g/cm$^3$. The microcanonical ensemble (NVE) is first used for 1 ns relaxation to balance the system, and then for 10 ns calculation. Since the reaction molecular dynamics simulation cannot complete the simulation calculation of plasma, we need to construct an equivalent model.

As ICP transmits a large amount of energy to the fused silica surface, the atoms in the outer layer instantly obtain extremely high energy. Therefore, we construct the equivalent model shown in Fig. 3 (b), where the colour corresponds to the atomic "theoretical temperature" (i.e., the kinetic energy of a single atom). The outermost atoms (5 layers) on the whole surface of the equivalent model are high-energy atoms, and the subsequent simulation calculation is carried out. The corresponding ICP plasma energy density can be obtained by setting the theoretical temperature. The conversion Formula (1) shows:

$$T - T0 = \frac{2\sum E_K}{d\hat{A}\cdot N\hat{A}\cdot K_B} \quad (1)$$

T is the theoretical temperature set for each atom, and $T_0$ is room temperature (300 K). $E_K$ is the kinetic energy of high-energy atoms compared with normal atoms. d is a spatial dimension (d = 3 in three-dimensional space). N represents the number of high-energy atoms. $K_B$ is the Boltzmann constant of 1.3806504 × $10^{-23}$ J/K. The extra energy of these high-energy atoms can be calculated by setting the theoretical temperature, which can be regarded as the energy transmitted by ICP plasma to the surface.

Fig. 4 (a) shows the Y-direction height model of the fused quartz surface after 20 ns of PAMM at different ICP energy densities. After

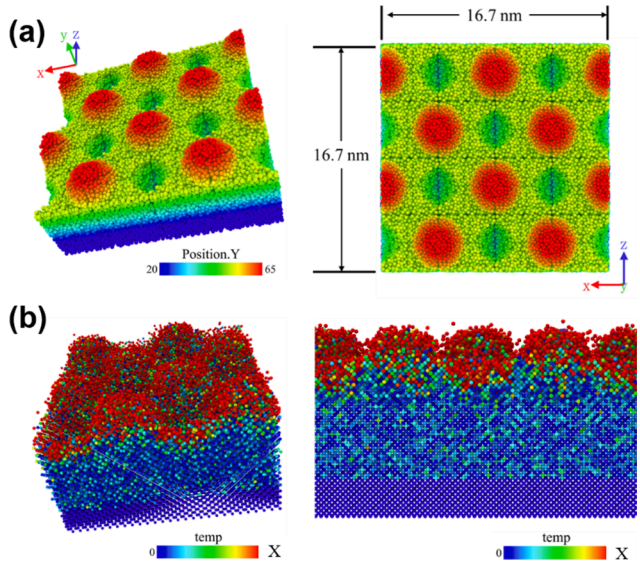


**Fig. 3.** Initial model of the fused silica surface. a) Height distribution model in the Y direction; b) equivalent temperature distribution model.

PAMM, the bulge and pit structures on the fused silica surface changed to varying degrees, and the height difference decreased significantly. Moreover, the surface morphology is directly related to the ICP energy density. While the ICP energy density is less than 73.18 eV/nm$^2$, bulges and pits still exist. With the increase in ICP energy density, the height difference is gradually reduced, and the structures of bulges and pits are gradually blurred. As the ICP energy density reaches 73.18 eV/nm$^2$, the bulges and pits on the fused silica surface almost completely disappear, forming a flat surface. When the ICP energy density is higher than 73.18 eV/nm$^2$, the bulges and pits in the initial surface model disappear, but irregular bulges are formed, affecting the smoothness of the surface. The PAMM effect of the fused quartz surface is closely related to the energy density of the ICP plasma. When the energy density is insufficient, the surface cannot obtain enough energy to complete the migration of atoms at all bulge positions. When the energy density is overloaded, the surface obtains excess energy and forms a new rough structure on the surface. Fig. 4 (b) shows the surface Sa roughness and temperature variation of fused silica corresponding to the ICP energy density. With increasing energy density, the Sa roughness shows the following trend: Sa first decreases gradually and then reaches the lowest value (less than 0.2 nm) in the range of 67.55–78.81 eV/nm$^2$. With the continuous increase in energy density, Sa roughness increases instead. This is consistent with the configuration variation of the fused silica surface shown in Fig. 4(a). In addition, there is an approximately linear relationship between the surface temperature and the energy density of ICP plasma, which means that the total internal energy of the system directly corresponds to the energy transmitted by ICP plasma.

To further analyse the variation in the surface structure of fused silica during PAMM, the Y-direction height model of the surface at an energy density of 73.18 eV/nm$^2$ is displayed in Fig. 5 (a). With the continuous progress of PAMM, the bulges and pits on the fused silica surface gradually disappear, and finally, a smooth surface structure is formed. As shown in Fig. 5 (b), the Sa roughness of fused silica decreases continuously and tends to be stable after approximately 8 ns (less than 0.2 nm). Root mean square deviation (RMSD) is the total displacement of all atoms in the system relative to the initial position. With the continuous progress of PAMM, the RMSD value increases and stabilizes after approximately 8 ns. Fig. 5 (c) shows the changes in surface tension and surface energy during PAMM. Because the fused silica surface is solid in the initial state, the surface energy and surface tension are extremely large. When the surface receives plasma energy from the micromelting state, the surface energy decreases greatly in an instant, and the interaction between the surface atoms is largely invalid. When the surface completely forms a micromelting state, the surface energy decreases slowly and stably, indicating that atomic migration on the fused silica surface is carried out stably and towards a trend of decreasing surface energy. Similarly, the surface tension exhibits a rapid and instantaneous reduction process. However, when the surface completely forms a micromelting state, the surface tension of fused silica increases slowly. Surface tension represents the force reducing the surface area for the micromolting state, so a gradual increase in surface tension corresponds to a gradual flattening of the surface structure.

To analyse the atomic migration in the PAMM process in detail, the XZ cross section of fused silica is observed and calculated, as shown in Fig. 6 (a). Fig. 6 (b) shows the force vector of the outermost atom on this XZ section at the initial PAMM moment, namely, the moment when ICP acts on the surface. The four colours represent different vector directions. It can be found that the vector directions of atoms change according to position. For high point atoms, the vector direction is parallel to the surface tangent direction, and most atoms are forced along the tangent point to the low point position. For low point atoms, the vector direction points to the centre of the pit. For the atoms at the "mountainside" position, there are two vector directions. On the one hand, the vector directions of some atoms are along the tangent. On the other hand, the volume of the fused silica surface expands after receiving energy, and the vector directions of some atoms are perpendicular to the

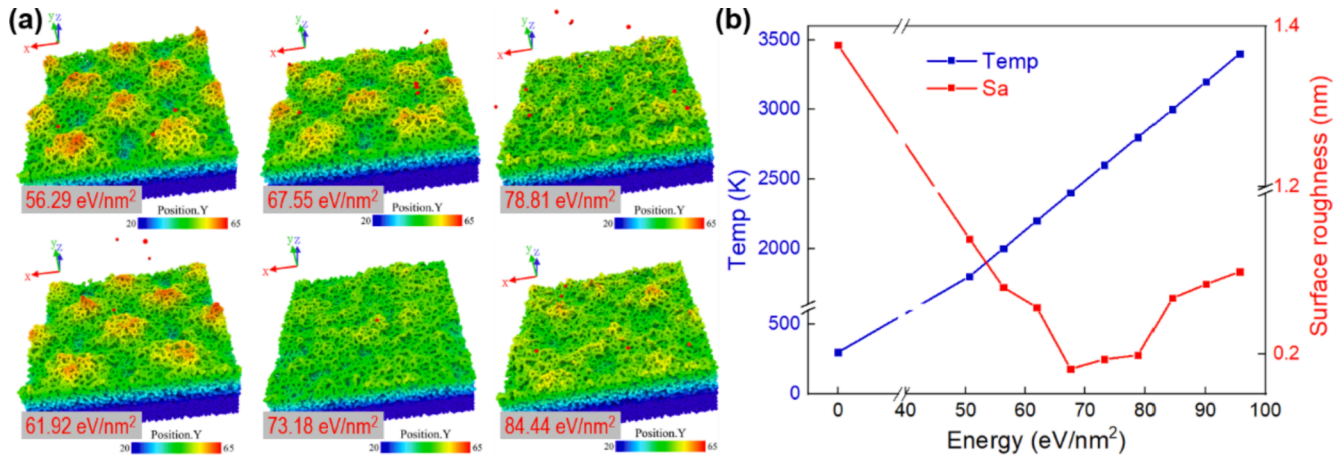


**Fig. 4.** a) Y-direction height model of the fused quartz surface after PAMM at different ICP energy densities; b) Sa roughness and surface temperature variation of fused silica versus ICP energy density.

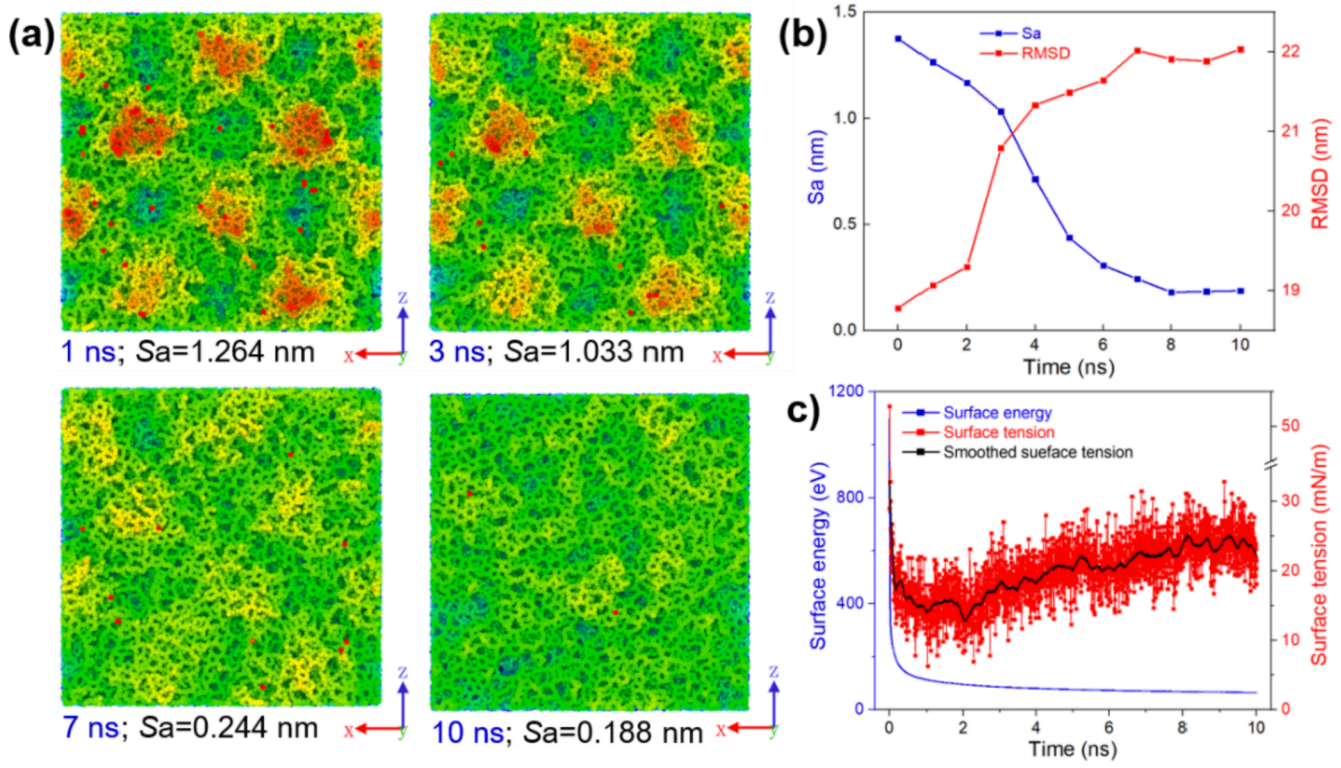


**Fig. 5.** Variation in the fused silica surface when the ICP energy density is 73.18 eV/nm$^2$: (a) Y-direction height; b) Sa roughness and RSMD; c) Surface energy and surface tension.

tangent direction, pointing to the centre of the pit. According to the results of vector analysis, the high point atom will migrate to the low point position, and the "mountainside" position atom and the low point atom will migrate to the pit centre position, which is consistent with our proposed atom migration discipline. Fig. 6 (c-d) shows the initial vector distribution on the fused quartz surface and the distribution after 10 ns of the PAMM process. When the ICP plasma acts on the surface at the initial time, the stress values at the high and low points are large, and the direction switches to the opposite. The stress distribution presents a stepped distribution from the high point to the low point. After PAMM, the distribution of surface stress is relatively disordered, and the magnitude of the stress value is significantly reduced, which indicates that the fused silica surface is in a relatively stable state.

Fig. 7 (a) shows the specific process of atomic migration on the fused silica surface with a two-dimensional bulge-pit structure during PAMM. Consistent with the calculation results in Fig. 6 (b), the atoms at the high point migrate to the low point, and the atoms at the "mountainside" position and the low point gather to the centre of the pit. After 20 ns of PAMM, two-dimensional fused quartz forms an ultrasmooth surface structure. Fig. 7 (b) shows the change in Ra roughness on two-dimensional fused silica, which decreased continuously with PAMM from 1.384 nm to below 0.2 nm. Since the fused silica is amorphous at the initial time, the value of the first neighbour atoms exhibits an obvious peak, but there is no obvious peak at the positions of the second and third neighbour atoms in the radial distribution function (RDF) curve of Si-O. After PAMM, the peak value of the first neighbour atoms decreases, but the second neighbour atoms has an obvious peak. This means that ordered structures begin to appear on the fused silica surface,

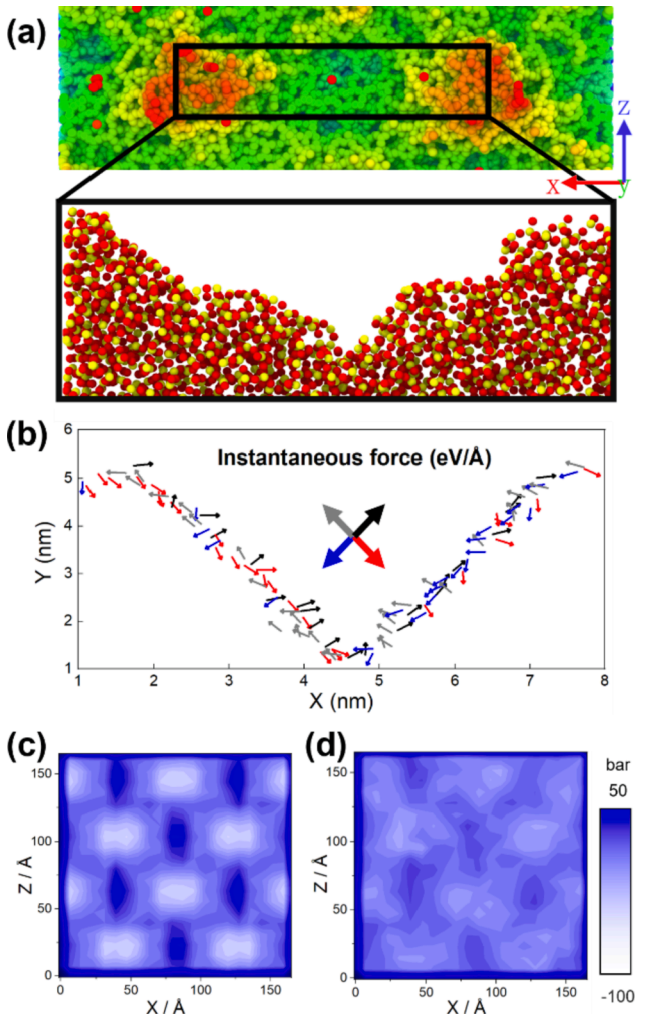


**Fig. 6.** a) Schematic diagram of the XZ cross-section of the fused silica surface; b) the initial force vector of the outermost atoms; the top view of the stress distribution of the fused silica when the ICP plasma intensity is 73.18 eV/nm$^2$ c) at the initial time and d) after PAMM completion.

and these ordered structures are obviously generated by atomic migration. Fig. 7 (d) shows the 12-element ring-like structure formed on the surface after PAMM, where the blue arrow represents the instantaneous force vector of the atom. According to the vector direction, these ring structures tend to form stable Si-O-12 rings, which means that the atoms in the outer layer are rearranged and tend to form an orderly regular structure. The order enhancement in the PAMM process is in accordance with the principle of energy minimization. Therefore, the atomic migration process on the fused silica surface will continue after ICP irradiation until an ultrasmooth surface is formed.

## 4. Experimental study of PAMM

The above molecular dynamics studies have theoretically proven the feasibility of PAMM to obtain an ultrasmooth fused silica surface and revealed the mechanism and activity of PAMM at the microscale. Based on theoretical research, the process of polishing fused quartz by PAMM was also studied. Fig. 8 (a) shows the physically fused quartz images before and after PAMM polishing. When the PAMM time is 10 min, the polished fused silica surface has a circular transparent area corresponding to the size of the plasma spot after the PAMM process. Fig. 8 (b) shows the boundary area of PAMM polishing. It can be found that the boundary between the polished and nonpolished areas is very clear, where the PAMM action area is obviously smooth. At the same time, a

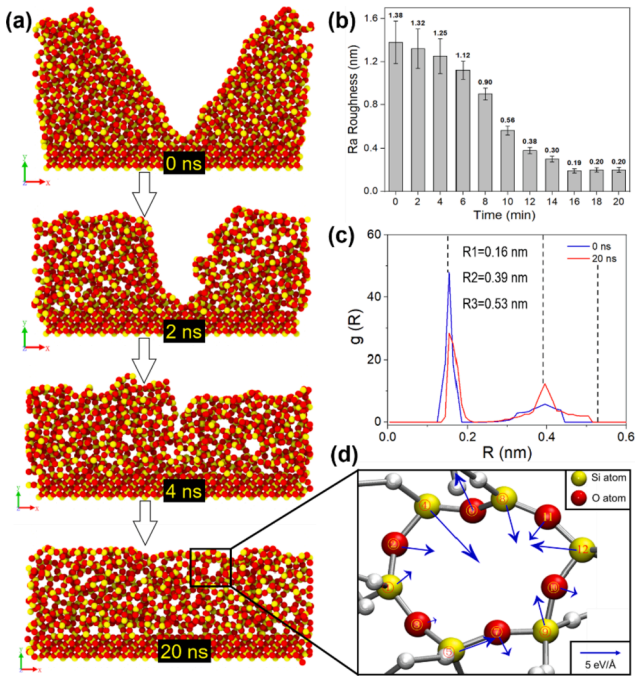


**Fig. 7.** a) Variation in the two-dimensional fused silica surface during PAMM; b) Ra roughness changes versus time; c) RDF curves of Si-O before and after PAMM; d) 12-element ring-like structure observed on the surface after PAMM.

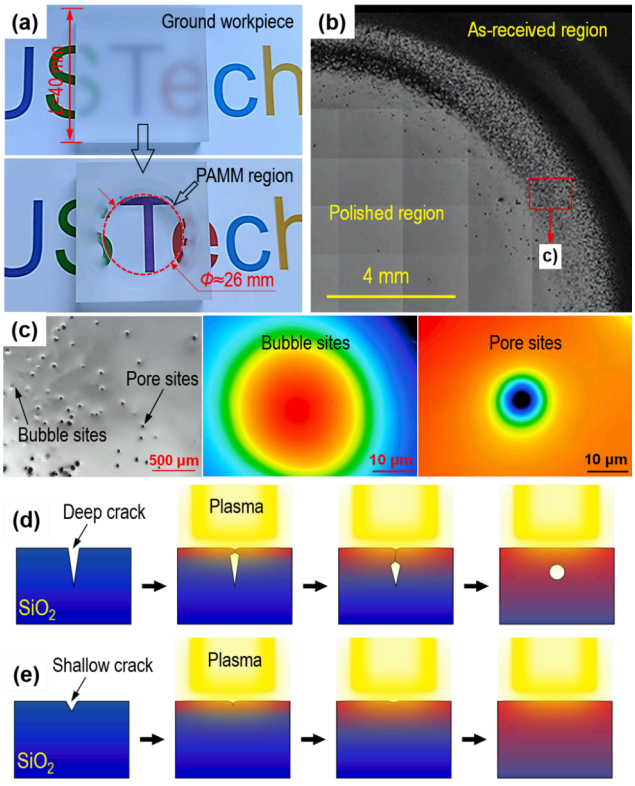


**Fig. 8.** (a) Fused quartz samples before and after PAMM; (b) LSCM diagram of the ICP irradiation boundary; (c) LSCM diagram of black spots, bubbles and pores in the PAMM polishing boundary region; (d) schematic diagram of the evolution process of deep cracks in the PAMM process; (e) schematic diagram of the healing process of shallow cracks in the PAMM process.

large number of black spots can be observed in the polishing boundary area, which seems to be the transition state from grinding to polishing. Fig. 8(c) further magnifies these black sites. The polished boundary area contains a large number of microprotrusions and microhole structures. From the laser confocal height image, the black sites can be divided into two types of structures: bubbles and pores. Fig. 8 (e-f) shows the formation mechanism of bubbles and pores. Considering the hard and brittle characteristics of fused silica, there are a large number of cracks with different depths on the ground surface. For deeper cracks, the edge region of the crack first extends and is directly closed to form a bubble structure due to uneven heating. The thermal expansion of bubbles may cause the formation of the bubble structure shown in Fig. 8 (c). Shallow cracks are gradually filled under the action of atomic migration and finally achieve the effect of crack healing. However, the shallow cracks that have not been healed exhibit the micron-level pore structure shown in Fig. 8 (c). Thus, PAMM can not only eliminate the roughness of the fused silica surface, but also exerts a good healing effect on the surface cracks.

There is no doubt that pores and bubbles on fused silica surfaces/subsurface have an effect on optical properties. The appearance of pores represents the transition state of PAMM, which can be completely eliminated in principle. However, the appearance of bubbles is closely related to the process parameters of the PAMM and the flow efficiency of surface atoms. Therefore, in subsequent research, it will be necessary to further explore the bubble elimination strategy in subsequent research.

To further study the variation in the surface morphology and roughness of fused silica during PAMM, the change process of the fused silica surface was analysed. Fig. 9 (a-b) shows the LSCM and AFM morphologies of the initial ground surface of fused silica. The ground surface is relatively rough, and the Sa roughness exceeds 450 nm. After 10 min of PAMM treatment, the fused quartz surface became smooth, and the Sa roughness measured by AFM was 0.17 nm, as shown in Fig. 9 (c-d). Fig. 9 (e) shows the surface roughness change versus time. After 1 min of PAMM, the surface roughness was greatly reduced to below Sa 60 nm. After PAMM for 8 min, the Sa roughness was further reduced and stabilized below 0.2 nm. It can be found that the PAMM not only achieves excellent subnanometre surface manufacturing accuracy, but also has outstanding roughness conversion efficiency. It is worth mentioning that the traditional optical manufacturing process often involves coarse abrasive mechanical polishing, fine abrasive mechanical polishing, MRF polishing and other auxiliary processes, such as cleaning and testing after grinding. In contrast, dry PAMM technology offers obvious advantages in polishing effect, roughness conversion efficiency and cost.

Fig. 9 (f) shows the change of the sample weights during the PAMM process. According to the basic principle of PAMM, the polishing effect of PAMM is based on the migration of atoms from high positions to low positions rather than the removal of materials. After a 10 min PAMM process, the weight loss of the material was less than 0.01%. This minute weight loss may be due to the instantaneous evaporation effect of a small amount of the outermost atoms when ICP irradiation impinges on the sample surface. Moreover, the working gas flow of ICP may also result in very little atomic removal.

In addition to the high-frequency roughness information, the low-frequency information of the surface also needs to be considered in optical manufacturing. In this study, AFM (5 μm), SWLI (400 μm) and stylus profilers (8 mm) were used to analyse the PAMM at different spatial frequencies. AFM is generally used to analyse the surface high spatial frequency roughness (HSFR). As shown in Fig. 10 (a) and (b), the effect of the PAMM on high-frequency roughness is obvious. In the SWLI image in Fig. 10 (b), it can be observed that the fused quartz has a continuous smooth surface after PAMM, corresponding to a decrease in the Sa roughness from 1.02 μm to 0.74 nm. It is worth noting that the PAMM-processed surface exhibits obvious fluctuations of 100 μm, and the specific formation mechanism is unclear. Considering the spot size of the plasma, the source of the 100 μm intermediate frequency error may be related to the surface shape error distribution of the initial ground surface. Fig. 10 also shows the surface profile and roughness curves before and after PAMM. After 10 min of PAMM, the Ra roughness of the fused silica surface decreased from 1.02 μm to 0.56 nm, reaching subnanometre roughness. However, it can also be found that there is an obvious millimetre-scale low-frequency fluctuation on the surface after

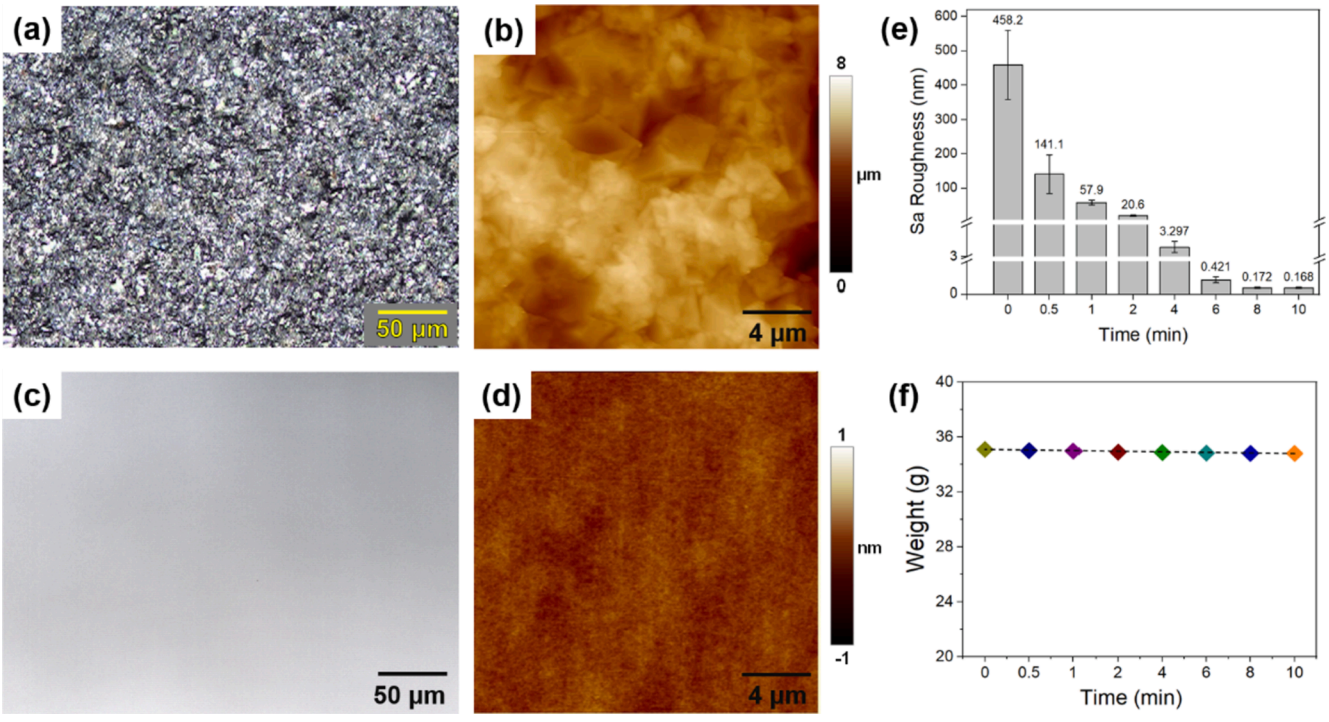


**Fig. 9.** LSCM images a) and AFM images b) of the fused silica surface before PAMM polishing; LSCM images c) and AFM images d) of the fused silica surface after PAMM polishing; e) Sa roughness changes versus time (10 min) on the fused silica surface during PAMM; f) sample weight changes versus time during PAMM.

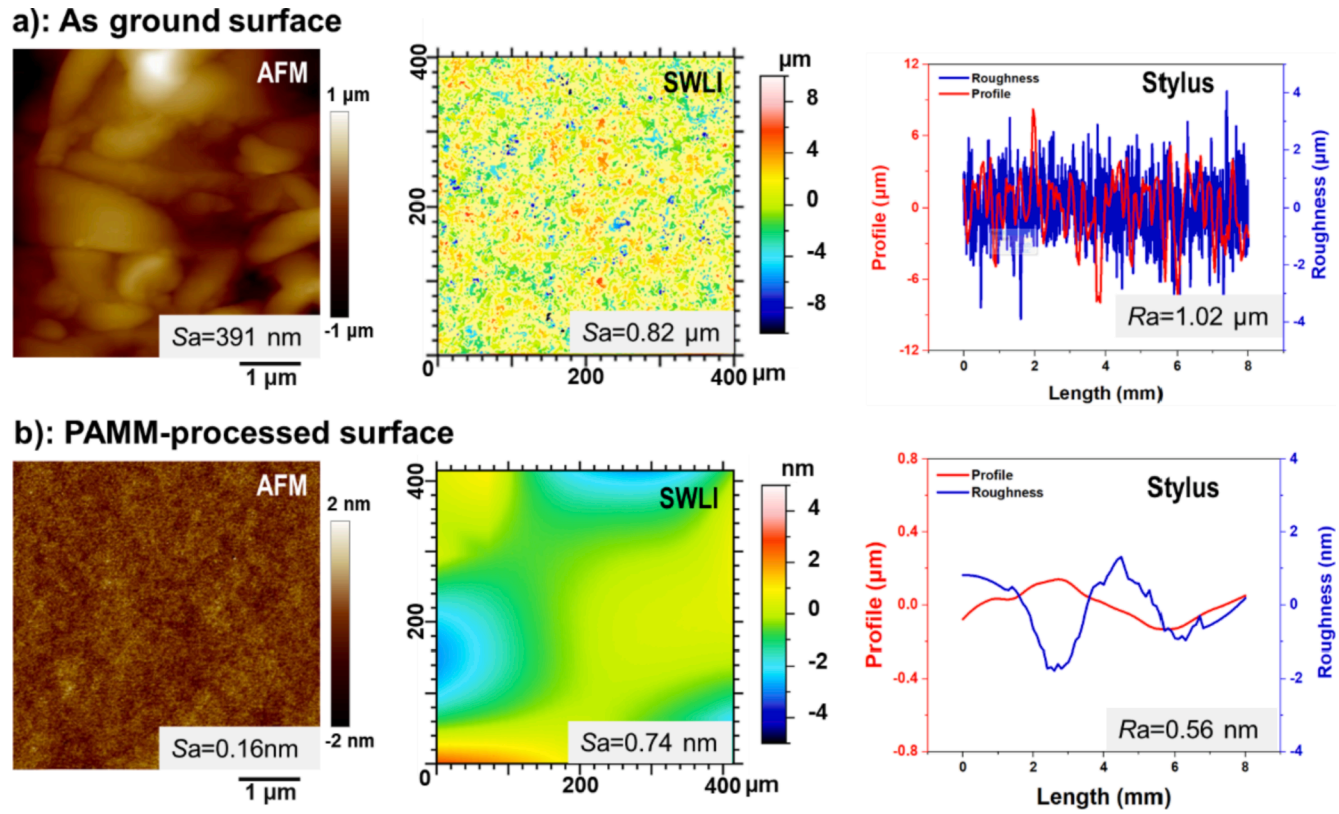


**Fig. 10.** Cross-scale analysis of fused silica surface before and after PAMM.

PAMM. During the PAMM process, due to the working gas flow effect of ICP plasma, the molten material on the surface may flow slightly. Whether the formation of low-frequency fluctuation is related to this remains to be further studied.

From the above results, it can be determined that PAMM technology can produce an ultrasmooth surface on the ground fused quartz sample with high efficiency, but the mechanism of PAMM in the mid/low frequency region is not clear. On the one hand, it is necessary to continue to explore the influence of PAMM on the surface shape error of optical components. It is obvious that PAMM does not offer modification ability, so it is worthy of further study to determine whether the surface roughness can be converted to the angstrom scale without affecting the surface shape. On the other hand, under the premise of only considering the excellent polishing ability of PAMM, the combination of PAMM and other modification processes can be explored.

Compared with the traditional "removal" polishing process, ultrasmooth surface manufacturing technology based on the energy beam-induced atom migration effect provides a new method for the transformation of ultraprecision optical manufacturing from the nanoscale to the angstrom scale. At present, PAMM technology still poses some engineering problems to be solved, such as the thermal stress problem under the action of ultrahigh temperature and the elimination of mid/low frequency errors. However, its high-efficiency angstrom-scale surface creation ability still has good development opportunities and application prospects [27]. PAMM principles and methods are similar to those of other energy beam surface technologies, but also exhibit unique characteristics. Different from electron beam [22,37] and ion beam [24,38] induced atomic migration manufacturing processes with the requirements of a vacuum environment, the PAMM process has a simpler operation and lower cost. The fused quartz sample can be polished directly in an atmospheric environment without limiting the sample size. Compared with laser polishing, less thermal stress is introduced and ablation particles are not generated. Compared with oxyhydrogen flame polishing, PAMM doesn't have the problem of OH contamination. Compared with the wet process based on polishing solution and magnetorheological fluids, such as CCOS and MRF, the PAMM dry polishing process offers obvious advantages in efficiency and cost. In summary, this work carried out a preliminary study on PAMM from the aspects of molecular dynamics simulation and plasma polishing experiments, hoping to provide a new ideal for future atomic-level ultraprecision optical manufacturing.

Although PAMM has demonstrated excellent surface smoothing capability, it is inapplicable for form error correction and the form accuracy may even deteriorate due to the thermal effect of ICP. Thus, the hybrid process combining PAMM with other figuring technologies such as MRF and CCOS will be developed in the future.

## 5. Conclusions

In this paper, molecular dynamics simulation and plasma polishing experiments are combined to study the polishing principle, process and characteristics of PAMM. The following conclusions can be drawn: ICP plasma exhibits the characteristics of high temperature, strong optical radiation and high ion concentration and is a method of inducing atomic migration comparable to the electron beam, ion beam and laser beam.

1. ICP plasma has the characteristics of high temperature, strong optical radiation and high ion concentration and is a method of inducing atomic migration comparable to the oxyhydrogen flame, electron beam, ion beam and laser beam.
2. The energy density transmitted by ICP plasma to the fused silica surface has a decisive influence on the polishing effect of PAMM. When the energy density is insufficient, complete migration of surface atoms cannot be achieved. When the energy density is overloaded, evaporation escape forms a new rough structure on the surface. Under the condition of an appropriate energy density, an ultrasmooth surface can finally be obtained.

3. Molecular dynamics simulation and PAMM polishing experiments show that an ultrasmooth surface with Sa roughness less than 0.2 nm can be obtained by PAMM technology. For a ground fused silica surface, Sa can be reduced from 458.17 nm to 0.17 nm by application of the PAMM process for 8 min, which proves the effectiveness and efficiency of PAMM as well as its broad applicable roughness range.
4. Although PAMM can efficiently obtain an ultrasmooth fused silica surface, it is ineffective with respect to the mid/low frequency error of the surface. The combination with other processing technologies with excellent shape control ability is the key breakthrough direction of the application of PAMM to optical manufacturing.

*CRediT authorship contribution statement*

**Shaoxiang Liang:** Data curation, Conceptualization, Methodology, Writing – original draft. **Linfeng Zhang:** Data curation, Validation, Methodology. **Hui Deng:** Conceptualization, Methodology, Project administration, Supervision.

## Declaration of Competing Interest

The authors declare that they have no known competing financial interests or personal relationships that could have appeared to influence the work reported in this paper.

## Acknowledgements

This work was partially supported by the National Natural Science Foundation of China (52005243, 52035009) and the Science and Technology Innovation Committee of Shenzhen Municipality (JCYJ20210324120402007, JCYJ20200109141003910). The authors acknowledge the assistance of the SUSTech Core Research Facilities.

## References

[1] R.A. Jones, Optimization of computer controlled polishing, Appl. Opt. 16 (1977) 218–224.
[2] B. Lin, K.L. Li, Z.C. Cao, T. Huang, Modeling of pad surface topography and material removal characteristics for computer-controlled optical surfacing process, J. Mater. Process. Technol. 265 (2019) 210–218.
[3] M. Kumar, A. Kumar, A. Alok, M. Das, Magnetorheological method applied to optics polishing: A review, in, IOP Conference Series: Materials Science and Engineering, IOP Publishing (2020), 012012.
[4] T. Arnold, G. Böhm, R. Fechner, J. Meister, A. Nickel, F. Frost, T. Hänsel, A. Schindler, Ultra-precision surface finishing by ion beam and plasma jet techniques—status and outlook, Nucl. Instrum. Methods Phys. Res., Sect. A 616 (2-3) (2010) 147–156.
[5] T. Hänsel, F. Frost, A. Nickel, T. Schindler, Ultra-precision Surface Finishing by Ion Beam Techniques, Vak. Forsch. Prax. 19 (2007) 24–30.
[6] F. Fang, Atomic and close-to-atomic scale manufacturing: perspectives and measures, Int. J. Extreme Manuf. 2 (2020) 030201.
[7] P. Wang, J. Wang, F. Fang, Study on Mechanisms of Photon-Induced Material Removal on Silicon at Atomic and Close-to-Atomic Scale, Nanomanufact. Metrol. 4 (4) (2021) 216–225.
[8] D.M. Eigler, E.K. Schweizer, Positioning single atoms with a scanning tunnelling microscope, Nature 344 (6266) (1990) 524–526.
[9] M. Rashidi, R.A. Wolkow, Autonomous scanning probe microscopy in situ tip conditioning through machine learning, ACS Nano 12 (2018) 5185–5189.
[10] Y. Sugimoto, P. Pou, O. Custance, P. Jelinek, M. Abe, R. Perez, S. Morita, Complex patterning by vertical interchange atom manipulation using atomic force microscopy, Science 322 (5900) (2008) 413–417.
[11] S. Pennycook, M. Varela, M. Chisholm, A. Borisevich, A. Lupini, K. Van Benthem, M. Oxley, W. Luo, J. McBride, S. Rosenthal, Scanning transmission electron microscopy of nanostructures, The Oxford Handbook of Nanoscience and Nanotechnology (2010) 205–248.
[12] P.A. Temple, W.H. Lowdermilk, D. Milam, Carbon dioxide laser polishing of fused silica surfaces for increased laser-damage resistance at 1064 nm, Appl. Opt. 21 (1982) 3249–3255.
[13] L. Zhao, J. Cheng, M. Chen, X. Yuan, W. Liao, Q. Liu, H. Yang, H. Wang, Formation mechanism of a smooth, defect-free surface of fused silica optics using rapid CO2 laser polishing, Int. J. Extreme Manuf. 1 (2019), 035001.
[14] H. Zhou, H. Zhou, Z. Zhao, K. Li, J. Yin, Numerical Simulation and Verification of Laser-Polishing Free Surface of S136D Die Steel, Metals 11 (2021) 400.
[15] D.I. Proskurovsky, V.P. Rotshtein, G.E. Ozur, A.B. Markov, D.S. Nazarov, V. A. Shulov, Y.F. Ivanov, R.G. Buchheit, Pulsed electron-beam technology for surface modification of metallic materials, J. Vacuum Sci. Technol. A: Vacuum, Surf. Films 16 (4) (1998) 2480–2488.
[16] D. Wei, X. Wang, R. Wang, H. Cui, Surface modification of 5CrMnMo steel with continuous scanning electron beam process, Vacuum 149 (2018) 118–123.
[17] J. Murray, A. Clare, Repair of EDM induced surface cracks by pulsed electron beam irradiation, J. Mater. Process. Technol. 212 (2012) 2642–2651.
[18] J. Tokunaga, T. Kojima, S. Kinuta, K. Wakabayashi, T. Nakamura, H. Yatani, T. Sohmura, Large-area electron beam irradiation for surface polishing of cast titanium, Dent. Mater. J. 28 (2009) 571–577.
[19] A. Okada, Y. Uno, J. McGeough, K. Fujiwara, K. Doi, K. Uemura, S. Sano, Surface finishing of stainless steels for orthopedic surgical tools by large-area electron beam irradiation, CIRP Ann. 57 (2008) 223–226.
[20] A. Okada, Y. Okamoto, Y. Uno, K. Uemura, Improvement of surface characteristics for long life of metal molds by large-area EB irradiation, J. Mater. Process. Tech 214 (2014) 1740–1748.
[21] B. Rosa, P. Mognol, J.-Y. Hascoët, Laser polishing of additive laser manufacturing surfaces, J. Laser Appl. 27 (S2) (2015) S29102.
[22] Z. Yu, Z. Wang, K. Yamazaki, S. Sano, Surface finishing of die and tool steels via plasma-based electron beam irradiation, J. Mater. Process. Technol. 180 (2006) 246–252.
[23] Y. Uno, A. Okada, K. Uemura, P. Raharjo, T. Furukawa, K. Karato, High-efficiency finishing process for metal mold by large-area electron beam irradiation, Precis. Eng. 29 (2005) 449–455.
[24] N.I. Chkhalo, S.A. Churin, M.S. Mikhaylenko, A.E. Pestov, V.N. Polkovnikov, N. N. Salashchenko, M.V. Zorina, Ion-beam polishing of fused silica substrates for imaging soft x-ray and extreme ultraviolet optics, Appl Opt 55 (2016) 1249–1256.
[25] E. Bourelle, A. Suzuki, A. Sato, T. Seki, J. Matsuo, Polishing of Sidewall Surfaces Using a Gas Cluster Ion Beam, Jpn. J. Appl. Phys. 43 (No. 10A) (2004) L1253–L1255.
[26] K.W. Lin, M. Mirza, C. Shueh, H.-R. Huang, H.-F. Hsu, J.v. Lierop, Tailoring interfacial exchange coupling with low-energy ion beam bombardment: Tuning the interface roughness, Appl. Phys. Lett. 100 (2012) 122409.
[27] T. Deng, J. Li, Z. Zheng, Fundamental aspects and recent developments in metal surface polishing with energy beam irradiation, Int. J. Mach. Tools Manuf 148 (2020), 103472.
[28] W. Dai, J. Li, Z. Zheng, Q. Huang, Surface finishing by atmospheric pressure micro plasma beam irradiation, Mater. Manuf. Processes 31 (2016) 1216–1222.
[29] T. Deng, F. Xie, J. Li, Z. Zheng, W. Zhang, Effect of overlapped adjacent tracks on surface morphology in plasma beam polishing of austenitic stainless steel, Appl. Surf. Sci. 512 (2020), 145739.
[30] T. Deng, J. Li, Z. Zheng, Micro-beam plasma polishing of ground alloy steel surfaces, Procedia Manuf. 15 (2018) 1678–1686.
[31] T. Deng, Z. Zheng, J. Li, Y. Xiong, J. Li, Surface polishing of AISI 304 stainless steel with micro plasma beam irradiation, Appl. Surf. Sci. 476 (2019) 796–805.
[32] B. FrantzDale, S.J. Plimpton, M.S. Shephard, Software components for parallel multiscale simulation: an example with LAMMPS, Eng. Comput. 26 (2) (2010) 205–211.
[33] W. Humphrey, A. Dalke, K. Schulten, VMD: Visual molecular dynamics, j mol graph 14 (1996) 33–38.
[34] A. Stukowski, Visualization and analysis of atomistic simulation data with OVITO–the Open Visualization Tool, Modelling Simul. Mater. Sci. Eng. 18 (2010) 2154–2162.
[35] J. Tersoff, New empirical model for the structural properties of silicon, Phys. Rev. Lett. 56 (1986) 632.
[36] B.W. Dodson, Development of a many-body Tersoff-type potential for silicon, Phys. Rev. B: Condens. Matter 35 (6) (1987) 2795–2798.
[37] A. Okada, Y. Uno, A. Iio, K. Fujiwara, K. Doi, New surface modification method of bio-titanium alloy by EB polishing, J. Adv. Mech. Des. Syst. Manuf. 2 (4) (2008) 694–700.
[38] A. Grobe, J. Schmatz, R. Littke, J. Klaver, J.L. Urai, Enhanced surface flatness of vitrinite particles by broad ion beam polishing and implications for reflectance measurements, Int. J. Coal Geol. 180 (2017) 113–121.